Published in final edited form as:

Curr Biol. 2022 February 07; 32(3): 545–558.e5. doi:10.1016/j.cub.2021.11.055.

Retinal horizontal cells use different synaptic sites for global feedforward and local feedback signaling

Christian Behrens[1,2,3,4], **Shubhash Chandra Yadav**[5,14], **Maria M. Korympidou**[1,2,4,14], **Yue Zhang**[1,2,4], **Silke Haverkamp**[6], **Stephan Irsen**[7], **Anna Schaedler**[1,2,4], **Xiaoyu Lu**[8], **Zhuohe Liu**[9], **Jan Lause**[1,2,3,4], **François St-Pierre**[8,9,10,11], **Katrin Franke**[1,2,3], **Anna Vlasits**[1,2,3], **Karin Dedek**[5], **Robert G. Smith**[8,12], **Thomas Euler**[1,2,3], **Philipp Berens**[1,2,3,13], **Timm Schubert**[1,2,*]

[1]Institute for Ophthalmic Research, University of Tübingen, Elfriede-Aulhorn-Str. 7, 72076 Tübingen, Germany

[2]Center for Integrative Neuroscience, University of Tübingen, Otfried-Müller-Str. 25, 72076 Tübingen, Germany

[3]Bernstein Center for Computational Neuroscience, University of Tübingen, Otfried-Müller-Str. 25, 72076 Tübingen, Germany

[4]Graduate Training Centre of Neuroscience, University of Tübingen, Otfried-Müller-Str. 27, 72076 Tübingen, Germany

[5]Neurosensorics/Animal Navigation, Institute for Biology and Environmental Sciences, University of Oldenburg, Carl-von-Ossietzky-Str. 9-11, 26111 Oldenburg, Germany

[6]Department of Computational Neuroethology, Center of Advanced European Studies and Research (caesar), Ludwig-Erhard-Allee 2, 53175 Bonn, Germany

[7]Electron Microscopy and Analytics, Center of Advanced European Studies and Research (caesar), Ludwig-Erhard-Allee 2, 53175 Bonn, Germany

[8]Systems, Synthetic, and Physical Biology Program, Rice University, 6500 Main St., Houston, TX 77005, USA

[9]Department of Electrical and Computer Engineering, Rice University, 6100 Main St., Houston, TX 77005, USA

[10]Department of Neuroscience, Baylor College of Medicine, One Baylor Plaza, Houston, TX 77030, USA

[*]corresponding author (timm.schubert@cin.uni-tuebingen.de), lead contact, Twitter handles: @teulerlab, @CellTypist.

Author contributions

Conceptualization, C.B., T.S. T.E and P.B., Methodology; Software; Validation; Formal Analysis C.B., S.C.Y., M.M.K. and J.L.; Investigation, C.B., S.C.Y., M.M.K., Y.Z., S.H., S.I., A.S. and T.S.; Resources X.L., Z.L., F.S-P. and R.G.S.; Data Curation, C.B., Y.Z., T.S.; Writing – Original Draft C.B. and T.S.; Writing – Review & Editing C.B., S.C.Y., M.M.K., S.H., F.S-P., K.F., A.V., K.D., R.G.S., T.E., P.B. and T.S.; Visualization, C.B., S.C.Y., M.M.K. and T.S.; Supervision, T.E., P.B. and T.S.; Project Administration, T.S.; Funding Acquisition, T.E., P.B. and T.S.

Declaration of Interest

The authors declare no competing interests.

[11]Biochemistry and Molecular Biology, Baylor College of Medicine, One Baylor Plaza, Houston, TX 77030, USA

[12]Department of Neuroscience, University of Pennsylvania, 422 Curie Blvd, Philadelphia, PA 19104, USA

[13]Tübingen AI Center, University of Tübingen, Maria-von-Linden-Straße 6, 72076 Tübingen, Germany

[14]these authors contributed equally

Summary

In the outer plexiform layer (OPL) of the mammalian retina, cone photoreceptors (cones) provide input to more than a dozen types of cone bipolar cell (CBC). In the mouse, this transmission is modulated by a single horizontal cell (HC) type. HCs perform global signaling within their laterally coupled network, but also provide local, cone-specific feedback. However, it is unknown how HCs provide local feedback to cones at the same time as global forward signaling to CBCs and where the underlying synapses are located. To assess how HCs simultaneously perform different modes of signaling, we reconstructed the dendritic trees of five HCs as well as cone axon terminals and CBC dendrites in a serial block-face electron microscopy volume and analyzed their connectivity. In addition to the fine HC dendritic tips invaginating cone axon terminals, we also identified “bulbs”, short segments of increased dendritic diameter on the primary dendrites of HCs. These bulbs are in a OPL stratum well below the cone axon terminal base and make contacts with other HCs and CBCs. Our results from immunolabeling, electron microscopy and glutamate imaging suggest that HC bulbs represent GABAergic synapses that do not receive any direct photoreceptor input. Together, our data suggests the existence of two synaptic strata in the mouse OPL, spatially separating cone-specific feedback and feedforward signaling to CBCs. A biophysical model of a HC dendritic branch and voltage imaging support the hypothesis that this spatial arrangement of synaptic contacts allows for simultaneous local feedback and global feedforward signaling by HCs.

eTOC Blurb

In the mammalian retina, it is unclear how horizontal cells provide both local feedback to photoreceptors and global forward signaling to bipolar cells simultaneously. Behrens *et al.* identify a second synaptic stratum in the outer mouse retina, spatially separating cone photoreceptor-specific feedback and feedforward signaling to bipolar cells.

Introduction

At the very first synapse of the mammalian visual system, retinal horizontal cells (HCs) play a crucial role in visual processing. They contribute to gain control, contrast enhancement, and the generation of center-surround receptive fields[1,3,4]. HCs are part of the circuit of the outer retina, where – in the mouse – the visual signal is transduced by two types of cone photoreceptors (cones) and relayed to 13 types of cone bipolar cell (CBC)[5–7]. These in turn forward the signal to the retina’s output neurons, the ganglion cells.

The laterally-organized HCs act on the mammalian photoreceptor-BC synapse[8] with a variety of feedback mechanisms[9–11]. To this end, HC dendritic processes invaginate cone axon terminals (also named ‘cone pedicles’) flanking ON-CBC dendrites to contact an individual cone output site in the synaptic cleft, forming a triad synapse[12] (Figure 1A). In contrast, HC dendritic tips do not directly contact OFF-CBCs at the cone axon terminal[13].

Despite the classic view that HCs are only involved in global feedback computations, recent functional measurements raised the possibility that HCs provide local feedback to photoreceptors at the triad synapse[14,15], modulating each cone’s output individually. Interestingly, an additional synaptic site from HCs to BCs below the cone terminals has been anecdotally observed in early electron microscopy (EM) studies of the vertebrate retina[16–18] and GABAergic feedforward connections between HCs and CBCs have been hypothesized[12,19–21]. Here, we integrate these seemingly disparate functions into a two-layer circuit of outer retinal processing in the mouse.

We made use of the serial block face EM dataset e2006[22] to reconstruct the mouse HC circuitry in the outer retina and identified a second synaptic layer formed with thickenings (“bulbs”) on HC dendrites, where HCs contact each other and BCs. Based on biophysical modeling, as well as glutamate and voltage imaging, we propose that a role of these synapses is to provide global feedforward signals to postsynaptic CBCs, complementing the local feedback provided directly to cones. This suggests that a single interneuron can simultaneously provide local reciprocal feedback and global feedforward signals at distinct synaptic locations.

Results

The connectivity of horizontal cells with cone photoreceptors

Using the publicly available serial block-face EM dataset e2006[22] (Figure 1B), we reconstructed the dendritic arbors of five HCs (Figure 1C and 1D). The reconstructed HCs covered a dendritic area of 4,600 ± 400 μm^2 (mean ± SD, n = 5). Typically, four to six primary dendrites originated from the soma and fine dendritic tips extended upwards towards cone axon terminals (Figure 1E). Note that for each of these HCs, a few distal dendrites could not be fully reconstructed, because they go beyond the EM tissue volume (Figure S1).

First, we analyzed the HC connectivity within the cone axon terminals (Figure 1F and 1G). We confirmed that connections between HCs and cones at this level of the OPL happened at the well-described “triad synapse”, where HC tips in the synaptic cleft are closely associated with invaginating dendrites of ON-CBCs[8] (Figure S2A). In our dataset, we identified one or two invaginating HC dendritic tips per ON-CBC tip in the synapses we analyzed (n=36). These synapses were located at five central cone axon terminals making contacts with all five reconstructed HCs.

Each HC contacted all cones within its (reconstructed) dendritic field, with on average 61 ± 5 (between 51 and 77) cones. We found that cones closer to the HC soma were contacted with more dendritic tips than distal cones (Figure 1F and S2B; Generalized Additive Model

(GAM) with smooth term for distance from soma and random effect of specific HC, $p < 2 \cdot 10^{-16}$ for smooth term, see STAR Methods). In addition, the HC-cone contact area decreased towards the HC's periphery (Figure 1G; GAM for distance from soma and random effect of specific HC, $p = 4.2 \cdot 10^{-7}$ for smooth term). As contact area may be a proxy for the probability of synaptic contacts[22], this suggests that HCs receive more synaptic input from cones close to their soma. Contacts between HCs and ON-CBCs at the level of the cone axon terminal followed the contact statistics between cones and ON-CBCs (Figure S3), as described earlier[7].

Horizontal cells and bipolar cells form contacts in the OPL

We next searched below the level of the cone axon terminals for an additional synaptic site between HCs and CBCs, which has been anecdotally described in early EM studies [16–19] and postulated based on physiological findings[12,20,21].

To this end, we systematically examined the five volume-rendered HCs and found dendritic thickenings distributed along the primary dendrites (Figure 2A and 2B). These dendritic thickenings, which we called "bulbs", showed a marked increase in dendritic diameter over the surrounding dendrite (Figure 2C). Almost all bulbs were located clearly below the cone axon terminal base and not in direct contact with it (Figure 2B and 2D). Also, the bulbs were evenly spread along the primary dendrites and across the entire dendritic field (Figure 2E and 2F) – in contrast to the number of invaginating dendritic tips, which showed a higher density towards the soma of the HC (cf. Figure 1F).

For 355 of the 545 mapped bulbs (n = 5 HCs) we could identify contacts with other neurons: 61.7% (219) only contacted the dendrites of ON- and OFF-CBCs, 18.9% (67) only contacted bulbs of other HCs, and 19.4% (69) contacted both HCs and CBCs, suggesting that the bulb structures represent potential HC-HC and/or HC-CBC synapses. For 190 bulbs, we could not determine the identity of the contacted cells as we had no information about the identity of the contacted cells: Only the five most complete HCs in the field were traced, and some CBCs had their soma outside the EM stack. Note that membrane boundaries between bulbs and other bulbs/BC dendrites in the 2006e EM data set were rather faint (Figure 2G and 2H). These faint boundaries were in stark contrast to other membranes in the OPL (see also Discussion).

On average, each HC contacted between 1 and 10 CBCs of a given type at bulb sites (Figure 2I). Most common were contacts to ON-CBC types 5O, 5I, 6 and 7; most rare, were contacts with types 1, 5T, X, 8 and 9. For types X, 8 and 9, the low numbers likely reflected these CBC type's lower density, whereas for CBC type 5T, which has the same dendritic density as CBC types 5O and 5I, it is likely a consequence of a genuinely lower number of contacts. From the CBCs' point of view, each ON-CBC contacted HCs on average at more than one bulb site (average: 1.1 to 2.2; except CBC type 5T), but OFF-CBC types at less than one (average 0.4 to 0.8; except CBC type 3A; Figure 2J). This indicates that HCs contact BCs in a type-specific manner at bulb structures below the cone axon terminal.

Horizontal cell bulbs are GABAergic synaptic structures

We next investigated whether these bulbs were indeed the site of GABAergic synapses from HCs to BCs. If this were the case, one would expect GABA receptors at the contact points between HC bulbs and CBC dendrites. To test this, we dye-injected six HCs and immunostained CBCs with antibodies against secretagogin (SCGN), which was described to label CBC types 2, 3, 4, 5, 6 and possibly 8[23]. In addition, we stained the tissue with antibodies against the GABA receptor subunit ρ2 (GABARρ2; Figure 3A and 3B), which in the lower OPL of the mouse is exclusively present on BC dendrites but not on cone axon terminals and HC primary dendrites[10,11,24,25].

We found GABARρ2-containing receptors at most HC bulbs (84%, 81 out of 96 bulbs, n = 6 HCs, Figure 3C and 3E). Moreover, GABARρ2 was present at more than half of the contact points (59%, 33 out of 56 contacts) between HC bulbs and SCGN-labelled dendrites of CBCs (58%, 56 out of 96 bulbs). Overall, almost one-third of the HC bulbs colocalized with both GABARρ2 and SCGN-labelled BCs (34%, 33 out of 96 bulbs). To assess whether these numbers were greater than expected by chance, we rotated the channel containing the dye-injected HC with respect to the SCGN and GABARρ2 channels by 90° and repeated the colocalization analysis (Figure 3D, see STAR Methods). We found that significantly fewer bulbs exhibited colocalization with the immunomarkers in the rotated condition (Figure 3E; $p<0.05$ for all conditions, Generalized Linear Mixed model, see STAR Methods and Table S1).

To evaluate if bulbs contain an ultrastructure consistent with synapses, we collected an image stack using focused ion beam scanning EM (see STAR Methods) on a sample where the intracellular ultrastructure was preserved (Figure 4). We manually reconstructed HCs starting from their dendritic tips in the invaginating cleft to the depth in the OPL, where bulbs are located (Figure. 4A and 4B, Supplementary image stack). While we were unable to detect synaptic vesicles (see Discussion), the bulbs always contained mitochondria, as is typical for presynaptic structures (Figure 4C and 4D, n = 7 bulbs)[26,27].

Together, our results from EM, dye-injections and immunolabelling support the view that HCs indeed form GABAergic synapses with CBCs at bulbs.

Horizontal cell bulbs are unlikely to receive direct photoreceptor input

In order to understand how synapses at HC bulbs might contribute to retinal processing, we turned to the question of how the retinal circuit could drive depolarization and GABA release from bulbs. First, we asked whether direct glutamatergic input from cones could locally depolarize bulbs. To evaluate this, we performed two-photon glutamate imaging in the transgenic $Cx57^{cre/+}$ mouse line[28], in which HCs expressed the genetically encoded glutamate sensor iGluSnFR[29] using AAV-mediated transduction (Figure 5; see STAR Methods). In the retinal whole-mount, we found localized, light-stimulus evoked glutamate signals in the OPL plane where the HC tips invaginate the cone axon terminals (Figure 5A, 5C and 5E) but not at HC bulbs (Figure 5B, 5D and 5F). This is confirmed by an analysis of response reliability with respect to light stimulation (see STAR Methods), which showed significantly higher reliability indices for signals at HC tips vs. bulbs (Figure

5G). To exclude the possibility that the lack of detectable glutamate signals at bulbs was due to the sequential nature of these recordings and, hence, photoreceptor bleaching, in a few experiments we used axial (x-z) scans[30], in which the whole OPL can be measured simultaneously (Figure S4). Like for the horizontal (x-y) scans, we detected reliable light-evoked glutamate signals only at the level of the cone axon terminals. Together, this suggests that glutamate released from photoreceptors does not diffuse to HC bulbs and contribute to depolarizing bulb compartments in a local manner. Thus, HC bulb GABA release can only be stimulated as a result of electrical signal spread along the primary dendrites and not from local glutamatergic drive from photoreceptors.

Biophysical modeling indicates potential bulb function

Given the lack of local glutamatergic input to bulbs, we next asked how electrical signals resulting from cone inputs are integrated at the HC bulbs in order to better understand the bulbs' functional response properties. To this end, we built a biophysical model of a HC dendritic branch with cone input (Figure 6A and 6B) based on our previously published model[15]. We stimulated the model with full-field noise, a spatially highly correlated input, and measured simulated voltage signals in the HC dendritic tips invaginating into cone axon terminals (n = 12) and in the bulb structures (n = 14) (Figure 6C and 6D). For full-field stimuli, we found high correlations between voltage signals from all recording points (0.79 ± 0.12, mean ± SD). Vesicle release at each synapse between cones and HC tip was modeled with a contribution from synaptic noise that was uncorrelated between synapses. Correlations between signals in different tips (0.64 ± 0.08) and between signals in tips and bulbs (0.77 ± 0.08) were therefore lower than those between signals in bulbs (0.92 ± 0.06) (Figure 6E and 6G). However, correlations between bulbs and the mean tip signals (0.95 ± 0.03) were similar to the correlations between bulbs. This suggests that even for full-field stimuli, signals in the tips are expected to be more independent than those in the bulbs.

We next stimulated the model with checkerboard noise, which is spatially uncorrelated. We found that the mean correlation between voltage signals in tips was low (0.20 ± 0.13), as reported previously[15]. In contrast, the mean correlation between voltage signals in bulbs was much higher (0.67 ± 0.21) and so was the correlation between bulb signals and the mean of tip signals (0.76 ± 0.11) (Figure 6F and 6G). Together, these simulations indicate the signal relayed by HCs to CBCs at the dendritic bulbs likely reports a de-noised spatial average of the visual stimulus, whereas the signals present at the HC dendritic tips consist of spatially-local information, providing spatially-local feedback to individual cones (Figure 7G and 7H).

Last, we ran simulations with larger bulbs (twice the bulb diameter) and without bulbs (bulb diameters reduced to that of the surrounding dendrite). Both conditions did not significantly change the calcium/voltage signals measurements at the bulb locations (Figure S5A). This is expected as the bulbs in our model have the same electric properties and channel densities as the surrounding primary dendrites. As the bulb only make up a small fraction of the HC dendritic length, signal propagation behavior is dominated by the properties of the dendrites between the bulbs. Moreover, assuming that bulbs indeed function as output synapses, we also ran models with increased voltage-gated calcium channel (VGCC) density solely in

the bulbs (Figure S5B). This modification did not significantly alter the signal correlations observed in different HC compartments.

Measuring membrane potential at the bulbs supports the biophysical model

To test the model's prediction that tip signals should be less correlated than bulb signals, we performed voltage imaging using JEDI-2P, a novel GFP-based genetically encoded voltage indicator (*manuscript submitted*) derived from ASAP2s[31]. JEDI-2P was expressed in HCs using AAV-mediated transduction in a transgenic $Cx57^{cre/+}$ animal (Figure 7; see STAR Methods). Similar to the glutamate recordings, voltage signals to full-field white flashes were recorded in x-y scans at the tip (Figure 7A and 7C) and the bulb level (Figure 7B and 7D). As predicted by our model (Figure 6G), flash-evoked voltage signals between different tips or tips and bulbs were less correlated than those between different bulbs, bulbs and somata or different somata (0.12 ± 0.01; 0.12 ± 0.01 vs. 0.16 ± 0.01; 0.19 ± 0.01; 0.24 ± 0.01; all mean ± 95% CI; Figure 7E and 7F), lending support to our model observation that bulbs relay more global aspects of the visual stimulus to their postsynaptic partners. Note that we also presented checkerboard noise stimuli, however, because of the low signal-to-noise ratio of the corresponding responses, we refrained from including these data into our analysis.

Discussion

Classically, HCs in the vertebrate retina have been viewed as performing global computations like gain control and contrast normalization[3,32,33]. However, local signaling in HC dendritic tips has also been observed[11,14,15], raising the question of how a strongly electrically coupled syncytium of laterally organized interneurons can compute both local and global signals and relay them to their postsynaptic partners. Here, we postulate an updated view of how HCs support these contrasting computations: HC dendritic tips provide local feedback – depending on the spatial stimulus properties – within the triad synapse in the cone terminal, directly modulating the cone output (Figure 7G), whereas GABAergic synapses at the HC dendritic bulbs relay a de-noised spatial average, or global spatial signal, of the visual signal to other HCs and to BCs (Figure 7H). This global output signal at the HC bulbs may play a role in generating the lateral surround of the center-surround receptive field of BCs, as has long been posited[34,35] (Figure 7I).

Horizontal cell bulbs as chemical synaptic structures

Based on anecdotal reports of chemical synapses between HCs and BCs in early EM studies in mammals[16–19], direct synaptic connections have long been postulated between HCs and CBCs in the vertebrate retina[12,20,21,36,37]. Our study reports segments of enlarged dendritic width – bulbs – in HCs and provides evidence that these bulbs are the putative HC-BC chemical synapses described over 30 years ago: First, contactivity analysis of reconstructed HCs and BCs indicates that the majority of bulbs (~65%) contact other HC and/or BC dendrites. That there appears to be type-specific wiring between CBC types and bulbs argues against these contacts being random en-passant contacts. Second, bulbs are regularly spaced along HC dendrites, suggesting that bulbs are not just random dendritic thickenings. Third, bulbs contain mitochondria, which are thought to be required in presynapses to

supply energy for the vesicle release mechanism, as described for a reciprocal amacrine cell synapse in the cat retina and cortical interneurons[27,38]. Fourth, our immunolabeling data indicates the presence of ρ2 subunit-containing $GABA_C$ receptors at HC bulbs that contact BC dendrites. Finally, using glutamate imaging, we did not detect any stimulus-modulated glutamate signal at the bulbs, which indicates that they do not receive direct glutamate input from cones.

While we were not able to directly detect neurotransmitter vesicles at HC bulbs (Figure 4), earlier EM studies found that vesicle clusters in HC dendrites were "…typically organized around some denser particles…" (Figure 18 in[17]) and that "…the synaptic complex, was of conventional configuration, involved the horizontal cell presynaptically, and was always found in the innermost aspect of the outer plexiform layer…" (Figure 11 in[16]). This is in line with our findings that bulbs are distributed in the inner stratum of the OPL. In a recent study, vesicles could be visualized in mouse HC tips in rod axon terminals using conical tomography EM with an isotropic voxel resolution of 3 nm[25,39]. Zampighi and coworkers[40] argued that together with an optimized fixation protocol, their high resolution approach eliminates possible projection artifacts seen in scanning block-face EM, which may mask fine cell organelle structures – such as small vesicles. Hence, potential explanations why we did not see any vesicles in both HC dendritic tips and bulbs in our EM datasets include sub-optimal fixation of the fine vesicles and/or masking artefacts from FIB-SEM imaging.

Another likely EM method-related observation was the rather indistinctive membrane boundary between bulbs and BC dendrites in the 2006e EM data set (Figure 2G and 2H). These faint boundaries were in stark contrast to other membranes in the OPL. Since we found bulbs with more intact-looking membranes to BCs in both dye-injected HCs and in our FIB-SEM tissue, the faint boundaries in the 2006e dataset are related to the staining protocol used at that time (compare Briggman, Helmstaedter and Denk 2011[41] with the optimized protocol in Fulton and Briggman 2021[42]).

It remains unclear whether HCs express GABA receptors at bulbs. This seems plausible as HCs contacted also other HCs at bulbs. A GABAergic synapse between HCs, along with depolarizing chloride levels in HCs[36,43], could transmit a sign-conserved signal between them, complementing the lateral signal spread through electrical synapses formed by gap junctions. It is unlikely that bulbs themselves are the primary site of gap junctions between HCs[44], as most of the gap junction protein connexin57 is expressed at more distal sites on the HC dendrites and not prominent on the bulb-bearing primary dendrites[45].

Functional consequences of a second synaptic stratum in the outer plexiform layer

Our findings suggest how the lateral inhibition essential for center-surround receptive field organization of BCs is generated by the HCs in the outer retina. While the thin distal HC dendrite appears to be optimized for local cone-specific feedback[15] (Figure 7G), the bulbs on the primary HC dendrites are particularly suitable for lateral inhibition: This GABAergic bulb synapse would relay global signals not only to other HCs but also to CBCs, where it could contribute to the cells' center-surround antagonistic receptive field. This feedforward signal to CBCs is likely modulated by different mechanisms: The photoreceptor input that reaches the bulbs on the primary HC dendrites will be shaped by the feedback at the

dendritic tip feedback synapses; in addition, it is subject to passive filtering and may be affected by the coupling state of the HC network, via electrical synapses and/or potential GABAergic synapses between HCs.

To provide both ON- and OFF-CBCs with the appropriate surround polarity, this GABAergic feedforward signal would need to have differential effects on the CBCs. Indeed, it has been found that ON- and OFF-CBCs differ in their dendritic Cl^- levels, such that activation of ionotropic GABA receptors, which are Cl^--permeable, results in Cl^- influx and hyperpolarization in OFF-CBCs and Cl^- efflux and depolarization in ON CBCs[21,37]. In this context it was puzzling that OFF-CBCs made fewer contacts with HC bulbs than ON CBCs. Here, a fundamental difference in ON- and OFF-CBC connectivity to cones may play a role: Whereas ON-CBCs invaginate the cone synaptic cleft and hence are closer to the glutamate release site, OFF-CBCs make basal contacts more distant from the release site and have to content themselves with less glutamate[46]. Therefore, the lower number of bulb contacts in OFF CBCs may counterbalance their reduced glutamatergic drive[47].

Another, - yet not investigated - factor that may contribute to the complexity of outer retinal signaling appears to be a tonic release of GABA by HCs on CBC dendrites that could modulate the CBCs' response to more phasic input from photoreceptors and/or HCs[11].

Feedback and feedforward signaling pathways

For spatially uniform light stimulation, local feedback from HCs to photoreceptors will approach the global averaged signal[48] (Figure 7G) and therefore, feedback to cones and the signal at the bulb synapse are expected to look similar. Under these conditions, however, the impact of a lateral component of global feedback from HCs to cones is expected to be relatively weak[2].

In contrast, for spatially patterned light stimulation, as can be expected during natural vision, the local feedback signal in the HC dendritic tips may look markedly different than the average signal generated in HC bulbs. Under these natural stimulation conditions, the local inhibitory feedback to cones may play an important role in locally boosting the signal-to-noise ratio of the signal by keeping the synapse at the optimal operating point[49]. Additionally, the global feedback signal, which represents the average background light intensity, has been suggested to support the optimal representation of (local) contrast signals[50].

However, feedback can also become unstable for high gains in the feedback loop and typical synaptic delays[2]. To prevent the initiation of such an oscillatory activity at the first synapse of the visual system, the HC feedback includes very fast, almost near instantaneous ephaptic/pH-mediated mechanisms with minimal delay following the cone signal[11,15,51]. Feedback strength is limited by the need to maintain efficient signal transmission from cones to CBCs. Note that global feedforward signaling at the HC bulbs does not suffer from such limitations. These functional requirements further constrain the feedback and feedforward synapses to be at structurally different synaptic sites (Figure 7I).

In addition, distinct synaptic mechanisms at the two synaptic sites – ephaptic/pH-mediated feedback and GABAergic feedforward signaling – may contribute to their different roles in the outer retina: The negative and positive feedback at the HC tip-to-cone synapse can decrease but also increase the cone output signal, respectively, depending on the stimulus context[2,10]. In contrast, the feedforward HC bulb-to-CBC synapse only provides a GABAergic drive. This signal provides inhibition to balance the excitation in CBCs, along with the activation of the spatial surround of the BC's receptive field.

The horizontal cell – an interneuron with multiple functions

HCs are not alone among interneurons in implementing distinct computations in a single neuron. Typically, this happens in a context-dependent manner: For example, in low light conditions, AII amacrine cells are central to the primary rod vision pathway, while under photopic conditions they change their role and contribute to approach sensitivity[52]. For A17 amacrine cells[53], which make reciprocal synapses with rod BCs, a functional switch between local and more global processing has been suggested[54]. Indeed, in the A17 amacrine cell-rod BC synapse, a plethora of transmitter-, voltage- and calcium-activated ion channels modulate inter-synaptic correlation of feedback from A17 amacrine cells to rod BCs[55–57]. The HC bulb differs in at least two ways: First, the A17 varicosity – as a typical reciprocal synaptic element – is both post- and presynaptic to the rod BC axon terminal. In contrast, HC bulbs are feedforward synapses to CBCs, likely without direct glutamatergic input – although they might be reciprocal synapses with respect to other HCs. Second, while A17 varicosities use a complex machinery to keep signal processing local (at least at low light levels), HC bulbs likely integrate signals from many tips arriving via the primary dendrites.

Note that AII and A17 amacrine cells likely fulfill either one or the other function – depending on the light level. However, there are also cases where interneurons perform different functions simultaneously: For instance, VG3 amacrine cells enhance motion sensitivity in several retinal circuits by providing excitatory and inhibitory drive at distinct synaptic sites[58,59]. Intriguingly, our findings suggest that HCs also fall into this category, as their feedback and feedforward signaling are apparently performed simultaneously at distinct synaptic sites via different synaptic mechanisms.

STAR Methods

Resource Availability

Lead contact

- Further information and requests for resources and reagents should be directed to and will be fulfilled by the lead contact, Timm Schubert (timm.schubert@cin.uni-tuebingen.de).

Materials availability

- This study did not generate new unique reagents.

Data and code availability

- This paper analyzes existing, publicly available data (see key resources data). Additional data used for this analysis has been deposited. DOIs are listed in the key resources table. All derived data used for data analyses is published together with the code (see https://github.com/berenslab/hc-connectivity). All other raw data reported in this paper will be shared by the lead contact upon request.
- All original code and data to rerun the analyses are available (see https://github.com/berenslab/hc-connectivity)
- Any additional information required to reanalyze the data reported in this paper is available from the lead contact upon request.

Experimental Model and Subject Details

All animal procedures were approved by the governmental review boards (Regierungspräsidium Tübingen, Baden-Württemberg, Konrad-Adenauer-Str. 20, 72072 Tübingen, Germany; Niedersächsisches Landesamt für Verbraucherschutz und Lebensmittelsicherheit, Martin-Niemöller-Straβe 2, 26133 Oldenburg, Germany; Landesamt für Natur, Umwelt und Verbraucherschutz Nordrhein-Westfalen, Leibnitzstraße 10, 45659 Recklinghausen) and performed according to the laws governing animal experimentation issued by the German Government. Owing to the exploratory nature of our study, we did not use randomization and blinding. No statistical methods were used to predetermine sample size.

For anatomical experiments (dye injection, immunolabeling), we used 3–6 month-old C57BL/6J mice of either sex. For the anatomical FIB-SEM experiments, a 14-week-old adult male C57BL/6J mouse was used. For two-photon imaging, we used 8 to 15-week-old $Cx57^{cre/+}$ mice of either sex (n = 3 for glutamate recordings; n = 1 for voltage recordings).

Method Details

Tracing in existing SBEM dataset—Our analysis is based on the scanning block-face EM (SBEM) dataset e2006[22] (https://www.neuro.mpg.de/connectomics). The dataset covers a piece of mouse retina of 132 × 114 × 80 μm with a resolution of 16.5 × 16.5 × 25 nm. We identified the somata of 15 HCs and skeletonized the dendrites of the five central HC using the software package KNOSSOS[60] (www.knossos.app). We used algorithms published with the dataset to reconstruct the volumes of HCs, BCs, and cone axon terminals in the OPL and to identify their contacts (for details see[7]).

We manually identified HC bulbs and their contacts. To compare the dendritic diameter profile around the bulbs with the one of random points on the dendrite (Figure 2C), we used the Vaa3D-Neuron2 auto-tracing[61,62] to get a simplified representation of the HC morphologies from the volume reconstruction, consisting of a regularly spaced grid of nodes with associated diameters. For each bulb position we identified the closest node and extracted the dendritic diameter profile around it. For a fair comparison to average points on the dendrite, we drew a random set of nodes with distributions of average distances from soma and tips matching the bulb locations.

To show that the bulbs are evenly distributed within the HC dendritic field, we compared the distribution of bulb nearest neighbor distances to that of random points (Figure 2F). For each HC, we drew as many random points on its dendrites as the cell had bulbs. We then calculated the nearest neighbor distances for both bulb and random point locations within each HC and plotted the binned nearest neighbor distances for all HCs.

To calculate the statistics of HC-to-BC contacts at bulbs, we included only BCs where the center of the BC dendritic field was within the dendritic field of at least one of the reconstructed HC. With this method, the numbers in Figure 2I and 2J are a lower bound. For the HCs, additional contacts on branches ending outside the dataset are possible as well as contacts from BCs with soma outside of the dataset, especially for larger types such as CBC types 8 and 9. The number of bulb contacts per CBC is also a conservative estimate, because the true coverage factor of HC dendrites is about 5–7, while we have only five overlapping HCs in the center and coverage is decreasing to ~1 towards the edges of the dataset.

Animals and tissue preparation—For anatomical experiments, animals were deeply anesthetized with CO2 and euthanized by cervical dislocation. Eyes were enucleated and instantly transferred to extracellular solution (in mM: 110 NaCl, 2.5 KCl, 1 CaCl2, 1.6 MgCl2, 10 glucose, 22 NaHCO3, adjusted to pH 7.4 witch 95% O2/5% CO2). Cornea, lens and vitreous body were removed, the retina was dissected from the eyecup and flat-mounted on filter paper, ganglion cells facing up.

For the anatomical FIB-SEM experiments, a 14-week-old adult male C57BL/6J mouse was deeply anesthetized with isoflurane and decapitated before the eyes were dissected. The posterior eyecups were immersion fixed in a solution containing 0.1 M cacodylate buffer, 4% sucrose and 2% glutaraldehyde, and then rinsed in 0.15 M cacodylate buffer.

For two-photon imaging experiments, animals were housed under a standard 12 h day/night rhythm at 22° C and 55% humidity. The viral construct AAV2.7m8.hSyn.iGluSnFR was generated by D. Dalkara (Inserm, Paris; Khabou et al. 2016), based on a plasmid construct provided by J. Marvin and L. Looger (Janelia Research Campus, USA). The viral construct AAV2/1-eF1α-DIO-JEDI-2P was generated by F. St-Pierre using the AAV expression plasmid developed here (see: Plasmid construction). A volume of 1 µl of the viral construct was then injected into the vitreous body in a mouse anaesthetized with 10% ketamine (Bela-Pharm GmbH & Co. KG) and 2% xylazine (Rompun, Bayer Vital GmbH) in 0.9% NaCl (Fresenius). For the injections, we used a micromanipulator (World Precision Instruments) and a Hamilton injection system (syringe: 7634-01, needles: 207434, point style 3, length 51 mm, Hamilton Messtechnik GmbH). Imaging experiments were performed 4 weeks after injection. Before the activity recordings, animals were dark-adapted for ≥1 h, then anaesthetized with isoflurane (Baxter) and killed by cervical dislocation. The eyes were enucleated and hemisected in carboxygenated (95% O_2, 5% CO_2) artificial cerebrospinal fluid (ACSF) solution containing (in mM): 125 NaCl, 2.5 KCl, 2 $CaCl_2$, 1 $MgCl_2$, 1.25 NaH_2PO_4, 26 $NaHCO_3$, 20 glucose, and 0.5 L-glutamine (pH 7.4). Then, the retina was flat-mounted on filter paper and was moved to the recording chamber, where it was continuously perfused with carboxygenated ACSF at ~36°C. All procedures were carried out under very dim red (>650 nm) light.

Horizontal cell injections and immunolabeling for secretagogin and GABA receptors—Six HCs were injected using Alexa Fluor 568 hydrazide (sodium salt in 200 mM KCl, Thermo Fisher, Karlsruhe, Germany)as described before[63]. In brief, cell nuclei in the retinal whole-mount preparation were visualized with DAPI labeling. Based on depth and size of the nuclei, HCs were identified and then injected with Alexa Fluor 568 using sharp electrodes and subsequently fixed with 4% paraformaldehyde. Retinal wholemounts were then incubated into primary and secondary antibodies for 7 and 2 days, respectively. GABARρ2 (rabbit, AGA-007, Alomone Labs, Jerusalem, Israel) and secretagogin (sheep, RD184120100, BioVendor, Brno, Czech Republic) polyclonal antibodies were used at a dilution of 1:500 and 1:1000, respectively. All steps were carried out at room temperature. All images were scanned with a Leica TCS SP8 confocal microscope using a 40x/1.3 oil objective. Data was deconvolved with Huygens Essential software (Scientific Volume Imaging, Hilversum, Netherlands), using a theoretical point spread function and further processed in Fiji[64]. Deconvolved stacks were normalized using stack histograms prior to colocalization analysis. Images were adjusted for brightness and contrast in Fiji for presentation purpose. Unless stated otherwise, images are shown as maximum projections of the z-stacks. However, the colocalization analysis (see next section) itself were carried out within each optical section.

Three-Dimensional Electron Microscopy using FIB-SEM—Focused ion beam-scanning electron microscopy (FIB-SEM tomography) allows efficient, complete, and automatic 3D reconstruction of HC dendrites with a resolution comparable to that of TEM[65,66]. A 1×1 mm^2 piece of a fixed C57BL/6J mouse retina (see Animals and tissue preparation) was stained in a solution containing 1% osmium tetroxide, 1.5% potassium ferrocyanide, and 0.15 M cacodylate buffer. The osmium stain was amplified with 1% thiocarbohydrazide and 2% osmium tetroxide. The retina was then stained with 2% aqueous uranyl acetate and lead aspartate. The tissue was dehydrated through an 70–100% ethanol series, transferred to propylene oxide, infiltrated with 50%/50% propylene oxide/Epon Hard, and then 100% Epon Hard. The Epon Hard block was hardened at 60°C.

Next, the block was prepared for FIB-SEM tomography. The sample was trimmed using an ultramicrotome (Leica UC 7) and afterwards glued onto a special sample stub (caesar workshop) using conductive silver paint. To avoid charge artifacts, all surfaces of the block were sputter-coated with 30 nm AuPd (80/20). A focused ion dual beam (FIB) workstation (XB 1540, Carl Zeiss Microscopy, Oberkochen, Germany) was used for tomogram acquisition. This instrument uses a focused gallium ion beam that can mill the sample at an angle of 54° with respect to the electron beam. A digital 24-bit scan-generator (ATLAS5, Carl Zeiss) was used to control ion and electron beam. The sample was milled using an ion beam of 1nA at an energy of 30 kV. Images were collected at an energy of 2 kV using a pixel size of 5×5 nm (x,y) and a layer thickness of 15 nm (z). Compared with resolution of the SBEM dataset 2006e ($16.5 \times 16.5 \times 25$ nm), the x,y resolution was increased by the factor 3.3 and 1.7, respectively. Milling and imaging was performed simultaneously to compensate for charging effects. The raw images were converted into an image stack, black areas were cropped, and the images were aligned using cross correlation[67]. HC dendrites were manually identified in ImageJ.

Plasmid construction—JEDI-2P (*manuscript submitted*) was cloned in a Cre-dependent (floxed) Adeno-Associated Virus (AAV) expression vector with the strong constitutive promoter eF1α (Addgene plasmid #20298). hChR2(H134R)-EYFP in the original vector was replaced with JEDI-2P using standard molecular biology techniques, resulting in the vector pAAV-eF1α-DIO-JEDI-2P (GenBank ID: in progress; Addgene plasmid #: in progress).

Two-photon glutamate and voltage imaging—We used a MOM-type two-photon microscope[68] (purchased from Sutter Instruments/Science Products). In brief, the system was equipped with a mode-locked Ti:Sapphire laser (MaiTai-HP DeepSee, Newport Spectra-Physics) to 927 nm, two fluorescence detection channels for iGluSnFR or JEDI-2P (HQ 510/84, AHF/Chroma) and SR101 (HQ 630/60, AHF), and a water immersion objective (W Plan-Apochromat ×20/1.0 DIC M27, Zeiss). We used custom-made image acquisition software (ScanM by M. Müller and T.E.) running under IGOR Pro 6.3 for Windows (Wavemetrics, Lake Oswego, USA), taking time-lapsed 128 × 128-pixel horizontal (x-y) scans (at 3.9 Hz) for glutamate and JEDI-2P imaging in the outer plexiform layer (OPL). For high resolution images, we used 512 × 512-pixel x-y scans. For axial (x-z) glutamate imaging in the OPL, we recorded time-lapsed 128 × 48-pixel x-z scans (at 13 Hz) using an electrically tunable lens[30].

For light stimulation, a DLP projector (lightcrafter (LCr), DPM-E4500UVBGMKII, EKB Technologies Ltd) with internal UV and green light-emitting diodes (LEDs) was focused through the objective (TTO)[69]. To optimize spectral separation of mouse M- and S-opsins, LEDs were band-pass filtered (390/576 Dualband, F59-003, AHF/Chroma). LEDs were synchronized with the microscope's scan retrace. Stimulator intensity (as photoisomerization rate, 10^3 P* per s per cone) was calibrated to range from ~0.5 (black image) to ~20 for M- and S-opsins, respectively. In addition, a steady illumination component of ~10^4 P* per s per cone was present during the recordings because of two-photon excitation of photopigments[68,70]. For all experiments, the tissue was kept at a constant mean stimulator intensity level for at least 15 s after the laser scanning started before light stimuli were presented. For glutamate imaging, two types of light stimuli were used: (1) full-field (700 μm in diameter) UV-green-white flashes, and (2) local (100 μm in diameter) chirp stimuli[71]. For voltage imaging, full-field white flashes were used.

Data analysis was performed using IGOR Pro. ROIs were defined automatically by custom correlation-based algorithms, as described before[72]. For glutamate imaging, the correlation threshold that was used to define ROIs at tip and bulbs level was 0.07 and 0.05, respectively. We used a lower threshold for bulbs because the overall correlations in these regions were lower. For voltage imaging, ROI size was restricted to 3 μm (in diameter) and a maximum of 6 pixels/ROI, at HC tips, bulbs, and somata. ROIs of bulbs and somata were separated manually based on a higher-resolution scan of the recorded anatomical structures. To measure the reliability of the ROI/pixel glutamate responses to the UV-green-white flashes and the chirp stimulus, we computed the signal-to-noise ratio, as described before[72,73]. To estimate the similarity between voltage traces, we computed the Pearson correlation coefficient.

Modeling—We built a biophysically realistic model of a HC dendritic branch using the simulation language NeuronC[74]. We used Vaa3D-Neuron2 auto-tracing[61,62] to generate a .swc file from the volume reconstruction of one HC branch and manually refined it in Neuromantic[75]. The model contains voltage-gated Ca^{2+} and K^+ channels with different channel densities for proximal and distal dendrites and AMPA-type glutamate receptors at the cone synapses (Table S2). Photoreceptors were modelled as predefined in NeuronC with two compartments including voltage-gated Ca^{2+} and Ca^{2+}-activated Cl^- channels. Cones were placed at the original positions with one synapse per invaginating HC dendritic tip found in the EM data. The synapses to the HC include postsynaptic AMPA channels modelled as Markov state-machines that included vesicle release noise. The model was stimulated for 60 s with both full-field and checkerboard Gaussian noise with a temporal frequency of 2 Hz and equal variance. The checkerboard stimulus consisted of independent pixels of 5 × 5 μm size such that all cones were stimulated independently. Voltage signals were recorded in a dendritic tip below each of the 12 cones and in 14 bulbs identified along the dendrite.

Quantification and Statistical Analysis

Colocalization analysis—Colocalization was defined as the signal overlap between the synaptic immunolabels (secretagogin and/or GABARρ2) and the dye-injected HCs. Areas with signal overlap in the HC stacks were determined by using the ‘colocalization highlighter’ plugin in Fiji[64] as described previously[76]. This plugin basically generates binary images highlighting overlapping regions where two channels of interest display values above a pre-determined threshold and a certain intensity ratio.

The three channels of interest were segmented using automatic-thresholds in Fiji. In principle, these thresholds classify signals in a stack into ‘objects’ and ‘background’. Stack histograms were considered for the segmentation step. Algorithms were chosen such that the segmented stacks best resembled the original deconvolved stacks. This was achieved by testing all the available algorithms in six HC stacks. ‘MaxEntropy’ and ‘Otsu’ was applied to HC and GABARρ2 channels, respectively. An average of ‘Default’ and ‘Li’ typically produced the best results for secretagogin channels and was accordingly chosen. The obtained threshold values were used to identify the colocalizing points between the two channels of interest. A default intensity ratio of 50% was set for all colocalization analyses. To determine colocalization between the three channels, the analysis was conducted sequentially: First, between HC and secretagogin, then between HC and GABARρ2, and finally, between the binary images obtained from the first two analysis. A threshold of 1 was used for the binary images.

The resulting binary images were merged with the original HC stack, thus projecting the colocalizing points onto the cell (Figure 3D). To minimize false-positive colocalization or overestimation, only an overlap of 10 connected voxels or larger was considered as truly colocalized (note that images were scanned at a voxel size of 47 × 47 × 170 nm). Next, the ‘3D Objects Counter’ Fiji plugin was used to identify objects larger than 10 voxels. Bulbs in the HC stacks were isolated by intersection of the HC channel with manually drawn masks around them. Finally, the bulbs with true colocalization were counted.

Finally, to rule out any chance-level colocalization, we repeated the colocalization analysis on the stacks with HC channel rotated clockwise by 90° relative to the GABARρ2 and secretagogin channels. To test for significance, we fitted for each marker condition the colocalization at individual bulbs as generalized linear mixed model with binomial output distribution and Wishart prior and fixed effect rotation and random effect HC identity using the R package *blme*. For all colocalization conditions the model shows rotation as a significant effect (Table S1).

To verify the colocalization detection, we repeated it with an additional method. Here, every bulb in the original HC stacks was visually inspected for potential colocalization within individual optical sections. A 2-μm line centered at the presumed colocalizing point was drawn in the merged RGB images[63]. Next, pixel intensities for the three channels of interest were plotted. If the intensity peaks of a pair of channels were separated by less than 0.25 μm, we considered this “true” colocalization. This colocalization threshold of 0.25 μm is about the maximum x-y resolution that can be achieved in our scanning conditions. The results obtained by both methods were consistent.

Statistics—Error bars in all plots are 95% confidence intervals (CIs) calculated as percentiles of the bootstrap distribution obtained via case resampling. In Figure 1F and 1G, we fitted generalized additive models[77] (R package *mgcv*) with Poisson output distribution for skeleton tips (Figure 1F) and Gamma output distribution for contact area (Figure 1G). Both had distance from soma as a smooth function and HC identity as smooth random effect. We used the two-sided Wilcoxon rank-sum test for quantifying difference in quality indices of glutamate traces between ROIs at the level of the HC tips and ROIs at the level of the primary dendrites.

To test for significant differences of the correlations shown in Figure 7E and 7F, we used a permutation test setup. With this test, we compared blocks of the correlation matrices shown in Figure 7E against each other. Each block showed the correlation of a set of source ROIs (rows) to a set of reference ROIs (columns). By construction, a block either represented within-ROI-type correlations (e.g. tips-to-tips), or between-ROI-type correlations (e.g. tips-to-bulbs). To summarize all correlations of a block, we took the average across its reference ROIs or columns, yielding a mean correlation for each source ROI. Next, we used those values to quantify the difference between two blocks by running a t-test on them. When the source ROIs were the same in both blocks, we used a paired-sample t-test. Otherwise, we used an independent two-sample t-test. This resulted in an empirical t-value. To test for significance, we obtained a null distribution over this t-value by permuting the ROI type labels of the traces and then repeating the above procedure 1,000 times, resulting in 1,000 t-values. Finally, we computed the p-value for the test as the percentile of the empirical t-value in the null distribution. To make the test two-sided, we used absolute t-values in all computation. The significance threshold was $p=0.05$.

We performed this test for all possible comparisons of within-type correlations (e.g. tips-tips vs. bulbs-bulbs). This amounts to comparing the blocks on the diagonal of the correlation matrix against each other, and always uses the independent t-statistic. All three tests were significant. Furthermore, for each ROI type, we compared its within-type correlations to its

correlations with other types. This means that we compared a block on the diagonal with an off-diagonal block. When comparing blocks above/below each other, the source ROIs were different, so we used the independent t-statistic. Of the six resulting tests, all were significant ($p < 0.001$) except for tips-tips vs. tips-bulbs ($p = 0.209$). When comparing blocks left/right to each other, the source ROIs in the compared blocks were identical, so we used the paired t-statistic. Of the six resulting tests, all were significant ($p < 0.001$) except for tips-tips vs. bulbs-tips ($p = 0.7$) and tips-tips vs. soma-tips ($p = 0.07$).

Supplementary Material

Refer to Web version on PubMed Central for supplementary material.

Acknowledgments

This work was supported by the German Research Foundation (DFG) through individual grants (SCHU2243/3-1 to TS and BE5601/6-1 to PB), a Heisenberg professorship (BE5601/4-1 to PB), the priority program SPP2041 (BE5601/2-1 to PB, EU 42/9-1 to TE), and the Excellence Cluster “Machine Learning – New Perspectives for Science (EXC 2064 – 390727645), the German Ministry of Education and Research through the Bernstein Award (FKZ 01GQ1601 to PB) and the Tübingen AI Center (FKZ 01IS18039A) and NIH grants (EY023766 to TE & RGS; EY022070 to RGS and R01EB027145 and U01NS113294 to F.S.-P.), the Klingenstein-Simons Fellowship Award in Neuroscience (F.S.-P.), the McNair Medical Foundation (F.S.-P.), Welch Foundation grant Q-2016-20190330 (F.S.-P.), and NeuroNex grant 1707359 (F.S.-P.)

We gratefully acknowledge Dr. Benjamin Arenkiel, Joshua Ortiz-Guzman, and Zihong Chen at the Texas Children’s Hospital Neuroconnectivity Core for packaging JEDI-2P in AAVs (this Core is supported by NIH grant P50HD103555 and the Charif Souki Fund) and Jonathan Oesterle for discussion.

References

1. Thoreson WB, and Mangel SC (2012). Lateral interactions in the outer retina. Prog. Retin. Eye Res. 31, 407–441. [PubMed: 22580106]
2. Smith RG (1995). Simulation of an anatomically defined local circuit: The cone-horizontal cell network in cat retina. Vis. Neurosci. 12, 545–561. [PubMed: 7654610]
3. Drinnenberg A, Franke F, Morikawa RK, Jüttner J, Hillier D, Hantz P, Hierlemann A, Azeredo da Silveira R, and Roska B (2018). How Diverse Retinal Functions Arise from Feedback at the First Visual Synapse. Neuron 99, 117–134.e11. [PubMed: 29937281]
4. Ströh S, Puller C, Swirski S, Hölzel M-B, van der Linde LIS, Segelken J, Schultz K, Block C, Monyer H, Willecke K, et al. (2018). Eliminating Glutamatergic Input onto Horizontal Cells Changes the Dynamic Range and Receptive Field Organization of Mouse Retinal Ganglion Cells. J. Neurosci. 38, 0141–17.
5. Wässle H, Puller C, Müller F, and Haverkamp S (2009). Cone contacts, mosaics, and territories of bipolar cells in the mouse retina. J. Neurosci. 29, 106–117. [PubMed: 19129389]
6. Tsukamoto Y, and Omi N (2014). Some OFF bipolar cell types make contact with both rods and cones in macaque and mouse retinas. Front. Neuroanat. 8, 105. [PubMed: 25309346]
7. Behrens C, Schubert T, Haverkamp S, Euler T, and Berens P (2016). Connectivity map of bipolar cells and photoreceptors in the mouse retina. Elife 5, 065722.
8. Haverkamp S, Grünert U, and Wässle H (2000). The Cone Pedicle, a Complex Synapse in the Retina. Neuron 27, 85–95. [PubMed: 10939333]
9. Liu X, Hirano AA, Sun X, Brecha NC, and Barnes S (2013). Calcium channels in rat horizontal cells regulate feedback inhibition of photoreceptors through an unconventional GABA- and pH-sensitive mechanism. J. Physiol. 591, 3309–3324. [PubMed: 23613534]
10. Kemmler R, Schultz K, Dedek K, Euler T, and Schubert T (2014). Differential Regulation of Cone Calcium Signals by Different Horizontal Cell Feedback Mechanisms in the Mouse Retina. J. Neurosci. 34, 11826–11843. [PubMed: 25164677]

11. Grove JCRR, Hirano AA, de los Santos J, McHugh CF, Purohit S, Field GD, Brecha NC, and Barnes S (2019). Novel hybrid action of GABA mediates inhibitory feedback in the mammalian retina. PLOS Biol. 17, e3000200. [PubMed: 30933967]
12. Yang X, and Wu S (1991). Feedforward lateral inhibition in retinal bipolar cells: input-output relation of the horizontal cell-depolarizing bipolar cell synapse. Pnas 88, 3310–3. [PubMed: 1849650]
13. Diamond JS (2017). Inhibitory Interneurons in the Retina: Types, Circuitry, and Function. Annu. Rev. Vis. Sci. 3, 1–24. [PubMed: 28617659]
14. Jackman SL, Babai N, Chambers JJ, Thoreson WB, and Kramer RH (2011). A positive feedback synapse from retinal horizontal cells to cone photoreceptors. PLoS Biol. 9.
15. Chapot CA, Behrens C, Rogerson LE, Baden T, Pop S, Berens P, Euler T, and Schubert T (2017). Local Signals in Mouse Horizontal Cell Dendrites. Curr. Biol. 27, 3603–3615.e5. [PubMed: 29174891]
16. Olney JW (1968). An electron microscopic study of synapse formation, receptor outer segment development, and other aspects of developing mouse retina. Invest. Ophthalmol. Vis. Sci. 7, 250–68.
17. Kolb H (1977). The organization of the outer plexiform layer in the retina of the cat: electron microscopic observations. J. Neurocytol. 6, 131–153. [PubMed: 856949]
18. Linberg KA, and Fisher SK (1988). Ultrastructural evidence that horizontal cell axon terminals are presynaptic in the human retina. J. Comp. Neurol. 268, 281–297. [PubMed: 3360989]
19. Dowling JE, Brown JE, and Major D (1966). Synapses of Horizontal Cells in Rabbit and Cat Retinas. Science (80-.). 153, 1639–1641.
20. Marchiafava PL (1978). Horizontal cells influence membrane potential of bipolar cells in the retina of the turtle. Nature 275, 141–142. [PubMed: 692683]
21. Duebel J, Haverkamp S, Schleich W, Feng G, Augustine GJ, Kuner T, and Euler T (2006). Two-Photon Imaging Reveals Somatodendritic Chloride Gradient in Retinal ON-Type Bipolar Cells Expressing the Biosensor Clomeleon. Neuron 49, 81–94. [PubMed: 16387641]
22. Helmstaedter M, Briggman KL, Turaga SC, Jain V, Seung HS, and Denk W (2013). Connectomic reconstruction of the inner plexiform layer in the mouse retina. Nature 500, 168–74. [PubMed: 23925239]
23. Puthussery T, Gayet-Primo J, and Taylor WR (2010). Localization of the calcium-binding protein secretagogin in cone bipolar cells of the mammalian retina. J. Comp. Neurol. 518, 513–525. [PubMed: 20020539]
24. Feigenspan A, and Weiler R (2004). Electrophysiological properties of mouse horizontal cell GABAA receptors. J. Neurophysiol. 92, 2789–2801. [PubMed: 15240758]
25. Hirano AA, Vuong HE, Kornmann HL, Schietroma C, Stella SL, Barnes S, and Brecha NC (2020). Vesicular Release of GABA by Mammalian Horizontal Cells Mediates Inhibitory Output to Photoreceptors. Front. Cell. Neurosci. 14, 600777. [PubMed: 33335476]
26. Gala R, Lebrecht D, Sahlender DA, Jorstad A, Knott G, Holtmaat A, and Stepanyants A (2017). Computer assisted detection of axonal bouton structural plasticity in in vivo time-lapse images. Elife 6, 1–20.
27. Turner NL, Macrina T, Bae JA, Yang R, Wilson AM, Schneider-Mizell C, Lee K, Lu R, Wu J, Bodor AL, et al. (2020). Multiscale and multimodal reconstruction of cortical structure and function. bioRxiv.
28. Ströh S, Sonntag S, Janssen-Bienhold U, Schultz K, Cimiotti K, Weiler R, Willecke K, and Dedek K (2013). Cell-specific cre recombinase expression allows selective ablation of glutamate receptors from mouse horizontal cells. PLoS One 8, 15–17.
29. Marvin JS, Borghuis BG, Tian L, Cichon J, Harnett MT, Akerboom J, Gordus A, Renninger SL, Chen T-W, Bargmann CI, et al. (2013). An optimized fluorescent probe for visualizing glutamate neurotransmission. Nat. Methods 10, 162–70. [PubMed: 23314171]
30. Zhao Z, Klindt DA, Maia Chagas A, Szatko KP, Rogerson L, Protti DA, Behrens C, Dalkara D, Schubert T, Bethge M, et al. (2020). The temporal structure of the inner retina at a single glance. Sci. Rep. 10, 4399. [PubMed: 32157103]

31. Chamberland S, Yang HH, Pan MM, Evans SW, Guan S, Chavarha M, Yang Y, Salesse C, Wu H, Wu JC, et al. (2017). Fast two-photon imaging of subcellular voltage dynamics in neuronal tissue with genetically encoded indicators. Elife 6.
32. Barnes S, Merchant V, and Mahmud F (1993). Modulation of transmission gain by protons at the photoreceptor output synapse. Proc. Natl. Acad. Sci. 90, 10081–10085. [PubMed: 7694280]
33. Verweij J, Kamermans M, and Spekreijse H (1996). Horizontal cells feed back to cones by shifting the cone calcium-current activation range. Vision Res. 36, 3943–3953. [PubMed: 9068848]
34. Werblin FS, and Dowling JE (1969). Organization of the retina of the mudpuppy, Necturus maculosus. II. Intracellular recording. J. Neurophysiol. 32, 339–355. [PubMed: 4306897]
35. Schwartz EA (1974). Responses of bipolar cells in the retina of the turtle. J. Physiol. 236, 211–224. [PubMed: 4818497]
36. Miller RF, and Dacheux RF (1976). Synaptic organization and ionic basis of on and off channels in mudpuppy retina. I. Intracellular analysis of chloride-sensitive electrogenic properties of receptors, horizontal cells, bipolar cells, and amacrine cells. J. Gen. Physiol. 67, 639–659. [PubMed: 932668]
37. Vardi N, Zhang L-L, Payne JA, and Sterling P (2000). Evidence That Different Cation Chloride Cotransporters in Retinal Neurons Allow Opposite Responses to GABA. J. Neurosci. 20, 7657–7663. [PubMed: 11027226]
38. Ellias SA, and Stevens JK (1980). The dendritic varicosity: a mechanism for electrically isolating the dendrites of cat retinal amacrine cells? Brain Res. 196, 365–372. [PubMed: 6249448]
39. Zampighi GA, Schietroma C, Zampighi LM, Woodruff M, Wright EM, and Brecha NC (2011). Conical Tomography of a Ribbon Synapse: Structural Evidence for Vesicle Fusion. PLoS One 6, e16944. [PubMed: 21390245]
40. Zampighi GA, Fain N, Zampighi LM, Cantele F, Lanzavecchia S, and Wright EM (2008). Conical Electron Tomography of a Chemical Synapse: Polyhedral Cages Dock Vesicles to the Active Zone. J. Neurosci. 28, 4151–4160. [PubMed: 18417694]
41. Briggman KL, Helmstaedter M, and Denk W (2011). Wiring specificity in the direction-selectivity circuit of the retina. Nature 471, 183–190. [PubMed: 21390125]
42. Fulton KA, and Briggman KL (2021). Permeabilization-free en bloc immunohistochemistry for correlative microscopy. Elife 10.
43. Kamermans M, and Werblin FS (1992). GABA-mediated positive autofeedback loop controls horizontal cell kinetics in tiger salamander retina. J. Neurosci. 12, 2451–2463. [PubMed: 1351934]
44. He S, Weiler R, and Vaney DI (2000). Endogenous dopaminergic regulation of horizontal cell coupling in the mammalian retina. J. Comp. Neurol. 418, 33–40. [PubMed: 10701754]
45. Janssen-Bienhold U, Trümpler J, Hilgen G, Schultz K, De Sevilla Muller LP, Sonntag S, Dedek K, Dirks P, Willecke K, and Weiler R (2009). Connexin57 is expressed in dendro-dendritic and axo-axonal gap junctions of mouse horizontal cells and its distribution is modulated by light. J. Comp. Neurol. 513, 363–374. [PubMed: 19177557]
46. DeVries SH, Li W, and Saszik S (2006). Parallel Processing in Two Transmitter Microenvironments at the Cone Photoreceptor Synapse. Neuron 50, 735–748. [PubMed: 16731512]
47. Turrigiano GG (2012). Homeostatic Synaptic Plasticity: Local and Global Mechanisms for Stabilizing Neuronal Function. Cold Spring Harb. Perspect. Biol. 4, a005736–a005736. [PubMed: 22086977]
48. Warren TJ, Van Hook MJ, Supuran CT, and Thoreson WB (2016). Sources of protons and a role for bicarbonate in inhibitory feedback from horizontal cells to cones in Ambystoma tigrinum retina. J. Physiol. 594, 6661–6677. [PubMed: 27345444]
49. Borghuis BG, Ratliff CP, and Smith RG (2018). Impact of light-adaptive mechanisms on mammalian retinal visual encoding at high light levels. J. Neurophysiol. 119, 1437–1449. [PubMed: 29357459]
50. Srinivasan MV, Laughlin SB, and Dubs A (1982). Predictive coding: a fresh view of inhibition in the retina. Proc. R. Soc. London. Ser. B. Biol. Sci. 216, 427–459. [PubMed: 6129637]
51. Vroman R, Klaassen LJ, Howlett MHC, Cenedese V, Klooster J, Sjoerdsma T, and Kamermans M (2014). Extracellular ATP Hydrolysis Inhibits Synaptic Transmission by Increasing pH Buffering in the Synaptic Cleft. PLoS Biol. 12.

52. Münch TA, Da Silveira RA, Siegert S, Viney TJ, Awatramani GB, and Roska B (2009). Approach sensitivity in the retina processed by a multifunctional neural circuit. Nat. Neurosci. 12, 1308–1316. [PubMed: 19734895]
53. Hartveit E (1999). Reciprocal Synaptic Interactions Between Rod Bipolar Cells and Amacrine Cells in the Rat Retina. J. Neurophysiol. 81, 2923–2936. [PubMed: 10368409]
54. Schubert T, and Euler T (2010). Retinal Processing: Global Players Like It Local. Curr. Biol. 20, R486–R488. [PubMed: 20541497]
55. Grimes WN, Hoon M, Briggman KL, Wong RO, and Rieke F (2014). Cross-synaptic synchrony and transmission of signal and noise across the mouse retina. Elife 3, e03892. [PubMed: 25180102]
56. Chavez AE, Grimes WN, and Diamond JS (2010). Mechanisms Underlying Lateral GABAergic Feedback onto Rod Bipolar Cells in Rat Retina. J. Neurosci. 30, 2330–2339. [PubMed: 20147559]
57. Grimes WN, Li W, Chávez AE, and Diamond JS (2009). BK channels modulate pre- and postsynaptic signaling at reciprocal synapses in retina. Nat. Neurosci. 12, 585–592. [PubMed: 19363492]
58. Lee S, Zhang Y, Chen M, and Zhou ZJ (2016). Segregated Glycine-Glutamate Co-transmission from vGluT3 Amacrine Cells to Contrast-Suppressed and Contrast-Enhanced Retinal Circuits. Neuron 90, 27–34. [PubMed: 26996083]
59. Tien NW, Kim T, and Kerschensteiner D (2016). Target-Specific Glycinergic Transmission from VGluT3-Expressing Amacrine Cells Shapes Suppressive Contrast Responses in the Retina. Cell Rep. 15, 1369–1375. [PubMed: 27160915]
60. Helmstaedter M, Briggman KL, and Denk W (2011). High-accuracy neurite reconstruction for high-throughput neuroanatomy. Nat. Neurosci. 14, 1081–1088. [PubMed: 21743472]
61. Peng H, Ruan Z, Long F, Simpson JH, and Myers EW (2010). V3D enables real-time 3D visualization and quantitative analysis of large-scale biological image data sets. Nat. Biotechnol. 28, 348–353. [PubMed: 20231818]
62. Xiao H, and Peng H (2013). APP2: Automatic tracing of 3D neuron morphology based on hierarchical pruning of a gray-weighted image distance-tree. Bioinformatics 29, 1448–1454. [PubMed: 23603332]
63. Yadav SC, Tetenborg S, and Dedek K (2019). Gap Junctions in A8 Amacrine Cells Are Made of Connexin36 but Are Differently Regulated Than Gap Junctions in AII Amacrine Cells. Front. Mol. Neurosci. 12, 1–15. [PubMed: 30809121]
64. Schindelin J, Arganda-Carreras I, Frise E, Kaynig V, Longair M, Pietzsch T, Preibisch S, Rueden C, Saalfeld S, Schmid B, et al. (2012). Fiji: an open-source platform for biological-image analysis. Nat. Methods 9, 676–682. [PubMed: 22743772]
65. Xu CS, Hayworth KJ, Lu Z, Grob P, Hassan AM, García-Cerdán JG, Niyogi KK, Nogales E, Weinberg RJ, and Hess HF (2017). Enhanced FIB-SEM systems for large-volume 3D imaging. Elife 6, 1–36.
66. Bosch C, Martí-nez A, Masachs N, Teixeira CM, Fernaud I, Ulloa F, Pérez-Martí-nez E, Lois C, Comella JX, DeFelipe J, et al. (2015). FIB/SEM technology and high-throughput 3D reconstruction of dendritic spines and synapses in GFP-labeled adult-generated neurons. Front. Neuroanat. 9.
67. Mastronarde DN (1997). Dual-Axis Tomography: An Approach with Alignment Methods That Preserve Resolution. J. Struct. Biol. 120, 343–352. [PubMed: 9441937]
68. Euler T, Hausselt SE, Margolis DJ, Breuninger T, Castell X, Detwiler PB, and Denk W (2009). Eyecup scope—optical recordings of light stimulus-evoked fluorescence signals in the retina. Pflügers Arch. - Eur. J. Physiol. 457, 1393–1414. [PubMed: 19023590]
69. Franke K, Maia Chagas A, Zhao Z, Zimmermann MJY, Bartel P, Qiu Y, Szatko KP, Baden T, and Euler T (2019). An arbitrary-spectrum spatial visual stimulator for vision research. Elife 8.
70. Euler T, Franke K, and Baden T (2019). Studying a Light Sensor with Light: Multiphoton Imaging in the Retina. In Multiphoton Microscopy, Hartveit E, ed. (Humana Press Inc.), pp. 225–250.
71. Szatko KP, Korympidou MM, Ran Y, Berens P, Dalkara D, Schubert T, Euler T, and Franke K (2020). Neural circuits in the mouse retina support color vision in the upper visual field. Nat. Commun. 11, 3481. [PubMed: 32661226]

72. Franke K, Berens P, Schubert T, Bethge M, Euler T, and Baden T (2017). Inhibition decorrelates visual feature representations in the inner retina. Nature 542, 439–444. [PubMed: 28178238]

73. Baden T, Berens P, Franke K, Román Rosón M, Bethge M, and Euler T (2016). The functional diversity of retinal ganglion cells in the mouse. Nature 529, 345–350. [PubMed: 26735013]

74. Smith RG (1992). NeuronC: a computational language for investigating functional architecture of neural circuits. J. Neurosci. Methods 43, 83–108. [PubMed: 1405746]

75. Myatt DR, Hadlington T, Ascoli GA, and Nasuto SJ (2012). Neuromantic – from Semi-Manual to Semi-Automatic Reconstruction of Neuron Morphology. Front. Neuroinform. 6, 1–14. [PubMed: 22319490]

76. Brüggen B, Meyer A, Boven F, Weiler R, and Dedek K (2015). Type 2 wide-field amacrine cells in TH::GFP mice show a homogenous synapse distribution and contact small ganglion cells. Eur. J. Neurosci. 41, 734–747. [PubMed: 25546402]

77. Wood SN (2017). Generalized Additive Models: An Introduction with R, Second Edition 2nd ed. (Chapman and Hall/CRC).

Highlights

- Horizontal cells show segments of increased diameter (bulbs) on their dendrites.
- Bulbs contact both bipolar cells and other horizontal cells.
- Bulb contacts are GABAergic synapses.
- Horizontal cells could provide global signals to bipolar cells at bulbs.

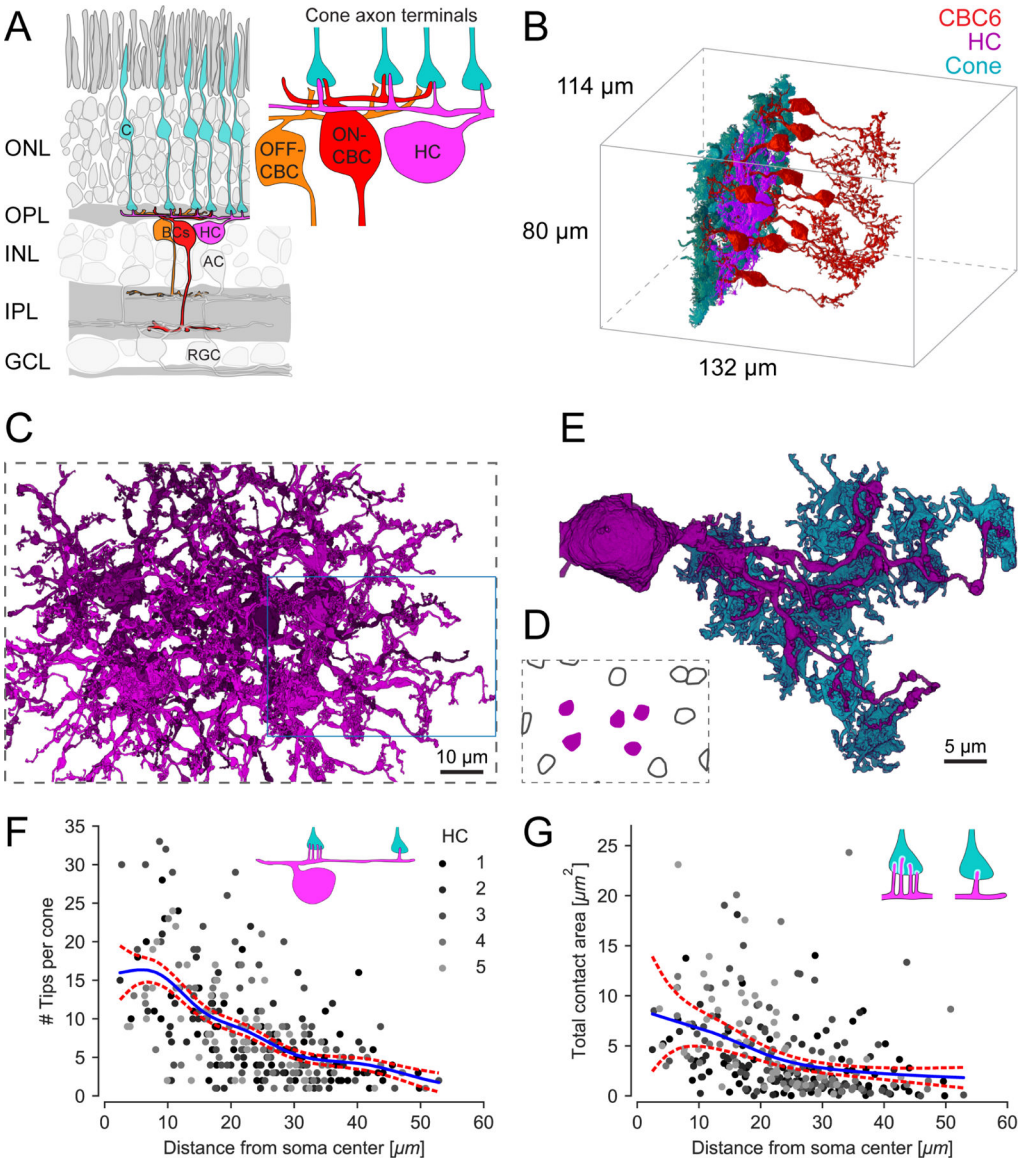

Figure 1. Horizontal cell reconstruction from electron microscopy data

(A) Schematic of a vertical section through the mouse retina, highlighting the reconstructed cell types. Inset: Textbook-view of the connectivity of bipolar cells (BCs) and horizontal cell (HC) at the cone (C) axon terminals with invaginating HC (magenta) and ON-CBC (red) dendritic tips and basal OFF-CBC contacts (orange). AC, amacrine cell; RGC, retinal ganglion cell. (B) Outlines of the dataset with volume reconstructed cone axon terminals (cyan), one HC (magenta) and several CBC type 6 (CBC6, red; only 10 of 45 CBC type 6 shown). (C) Volume reconstructions of five HCs (top view); blue rectangle: location of dendrite shown in (E). For renderings of the individual cells see Figure S1. (D) Soma locations of the five reconstructed HCs (magenta, shown in C) and 10 HCs not reconstructed (black outline). (E) Bottom view of the volume reconstruction of a complete single HC primary dendrite (magenta) with contacted cone axon terminals (cyan). HC dendrite taken from inset in (C). (F) HC skeleton tips per contacted cone vs. distance from HC soma. Blue:

Poisson GAM fit with 95%-confidence interval (red). Inset illustrates the number of HC tip-to-cone contacts at different locations along the HC dendrite. See Figure S2 for an example EM slice and HC branch skeleton. (G) Contact area between HC and cone axon terminal volume reconstructions per cone vs. distance from HC soma. Blue: Gamma GAM fit with 95%-confidence interval (red). Inset illustrates contact areas (white) for close-to-the-soma contacts (left) and more distant (right) contacts. For contact statistics between cones and ON-CBCs see Figure S3.

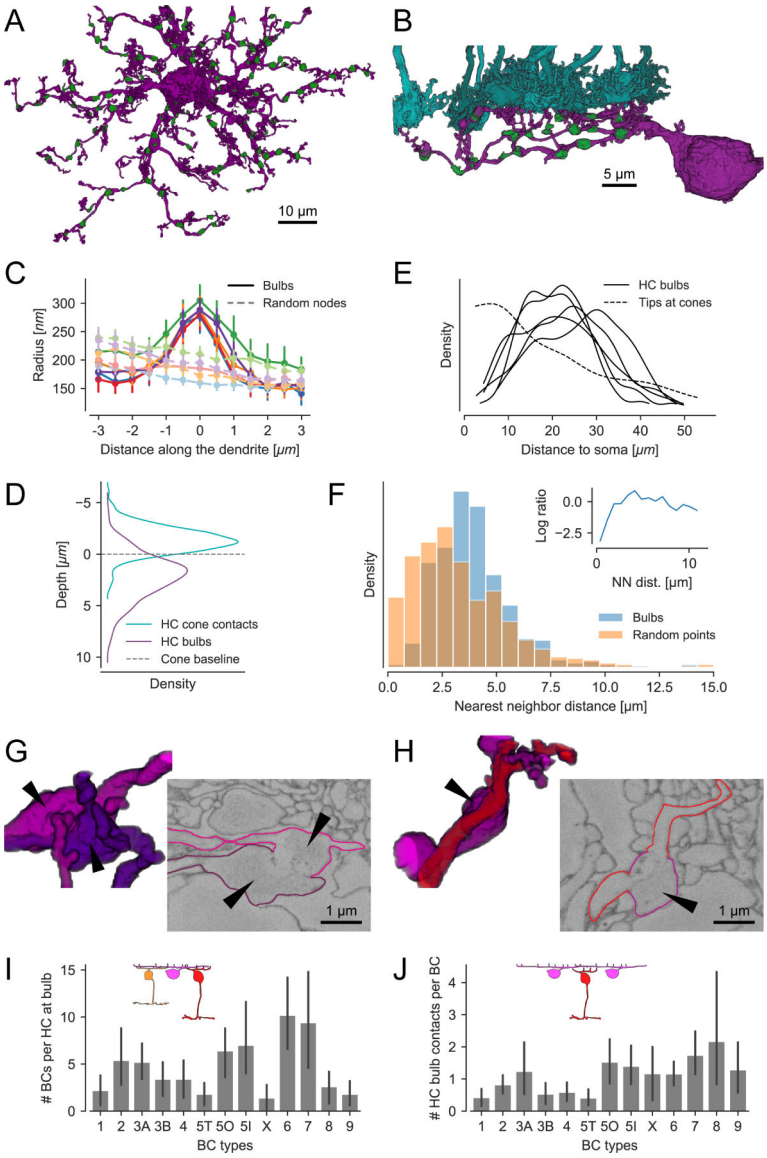

Figure 2. Identification and properties and contacts of “bulbs” in horizontal cells

(A) Top view of a reconstructed HC with bulbs highlighted in green. (B) Side view of a branch from the same HC with bulbs (green) and cone axon terminals (cyan). (C) Dendritic radius profile at bulb locations (solid curves w/high saturation) compared to randomized points on the dendrites (dashed curves w/low saturation). For each of the five reconstructed HCs we analyzed the distribution of distances from bulbs to soma and dendritic tips. We generated a set of random locations on the HC dendrites so that number and distribution of distances matches the bulb statistics. For both sets of points we extracted the dendritic radius in their vicinity and plotted the averages per HC. Color represents individual HCs; error bars show 95%-confidence intervals. Note that the radius gradually decreases with increasing distance due to the tapering of the dendrite. (D) Depth of bulbs compared to HC-cone contacts. (E) Kernel density estimate of the distance distribution of bulbs relative to the soma for all five HCs. Dashed curve: Model fit showing distribution of HC skeleton tips at cones

from Figure 2C. (F) Histogram of bulb nearest neighbor (NN) distances within individual HCs vs. the same number of points randomly distributed on the HC dendrites. Inset: Log ratio between bulb and random point NN distances. (G) Volume rendering and EM slice showing a bulb contact between two HCs. (H) Volume rendering and EM slice showing a contact between HC (magenta) bulb (arrowhead) and ON-CBC (red). (I) BCs contacted by bulbs per HC for all CBC types. (J) HC bulb contacts per BC for all CBC types. Likely, the number of contacts per CBC is underestimated since contacts to not reconstructed HCs are not included. All error bars show 95%-confidence intervals.

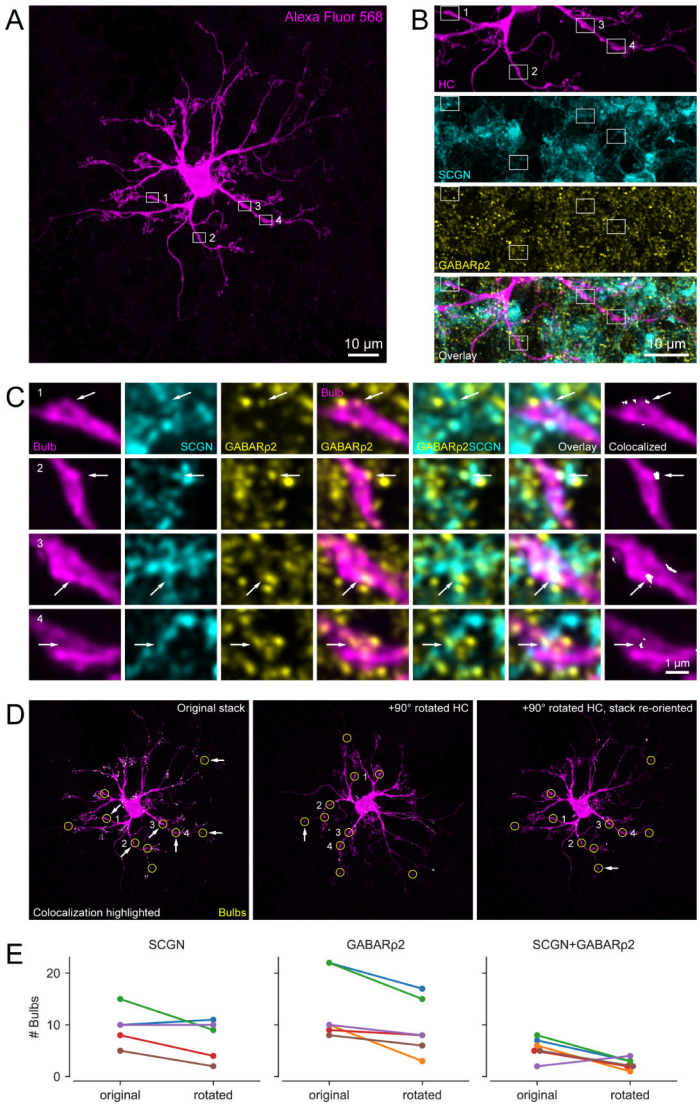

Figure 3. GABARρ2 receptors are present at the contact points between horizontal cell bulbs and CBC dendrites

(A) Alexa Fluor 568-injected HC with identified bulbs (white boxes indicate examples). Note that the brightness was increased for better visibility. (B) Magnified clipping from (A) showing four representative bulbs (magenta) as well as their corresponding secretagogin (SCGN, cyan) and GABARρ2 (yellow) stainings. The bottom panel represents overlay of the three channels. (C) Enlarged bulbs from boxes in (B) with SCGN and GABARρ2 immunolabeling. Both individual (columns 1–3) and merged channels (columns 4–6) are shown, with arrows indicating colocalization. Colocalization of all three channels at the bulbs (column 7) identified by ‘colocalization highlighter’ plugin in Fiji (see panel D). (D) Colocalizing points highlighted in original (left) and 90-degree rotated HC (center, right), with bulbs encircled (yellow). Arrows denote bulbs with colocalization. (E) Line plots showing number of bulbs (per HC, n = 6 HCs) colocalizing with SCGN (left), GABARρ2 (center) and both (right) for non-rotated (original) and 90-degree rotated condition, see also Table S1. Note that images are maximum projections: (A, D) of the entire HC stack

(85 optical slices), (B) of the selected clipping (40 optical slices), and (C) of 5–7 optical slices for better visibility of the bulbs. Optical section thickness was 0.17μm. Colocalization analysis itself were carried out within each optical section.

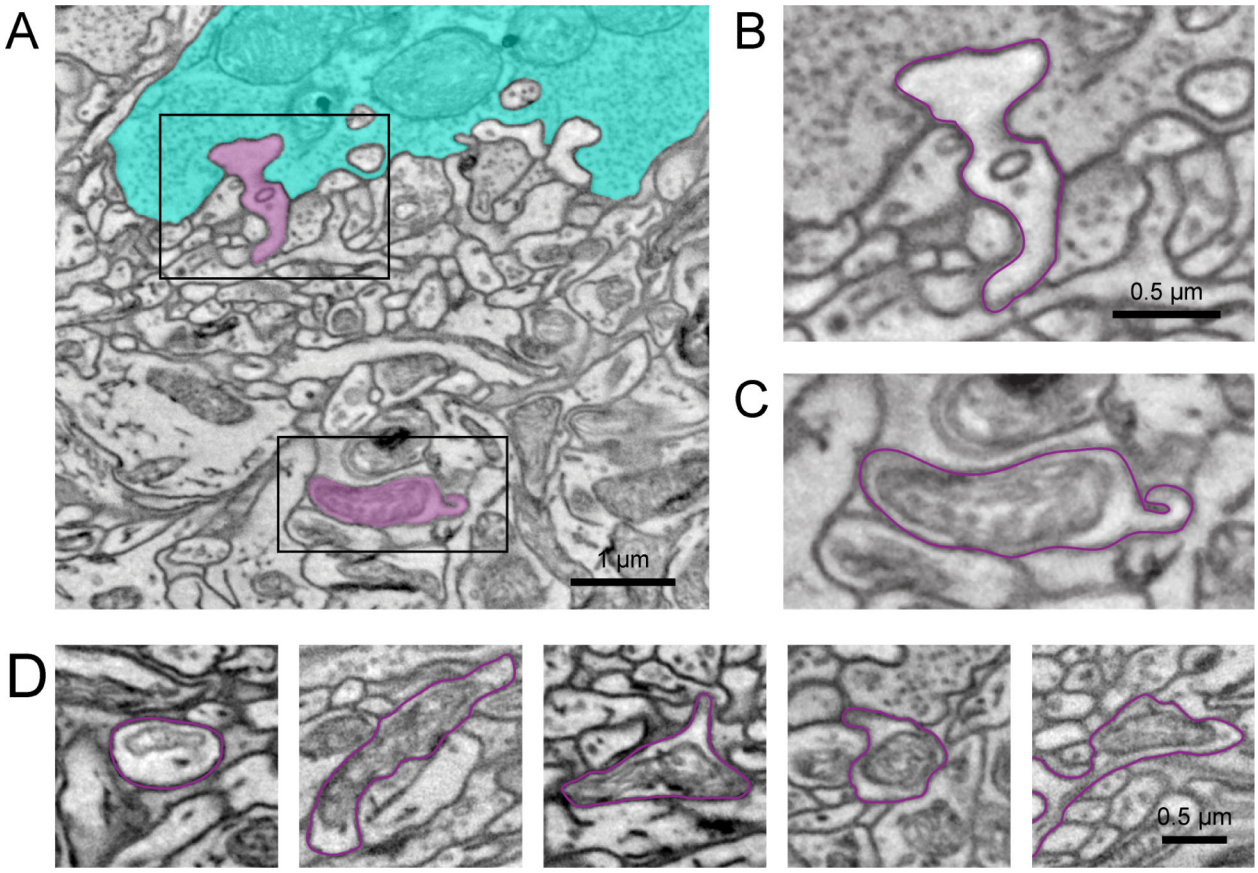

Figure 4. Mitochondrial structure in HC bulbs

(A) Electron micrograph showing a manually traced HC (magenta) with a dendritic tip invaginating in a cone axon terminal (cyan) (B) and the primary dendrite below the cone axon terminal with a HC bulb of the same cell (C). See also the Video S1 visualizing the complete EM stack. (D) Additional examples of HC bulbs (magenta outline). Note the mitochondrial structure in the bulbs. Black rectangles: location of magnifications shown in (B,C).

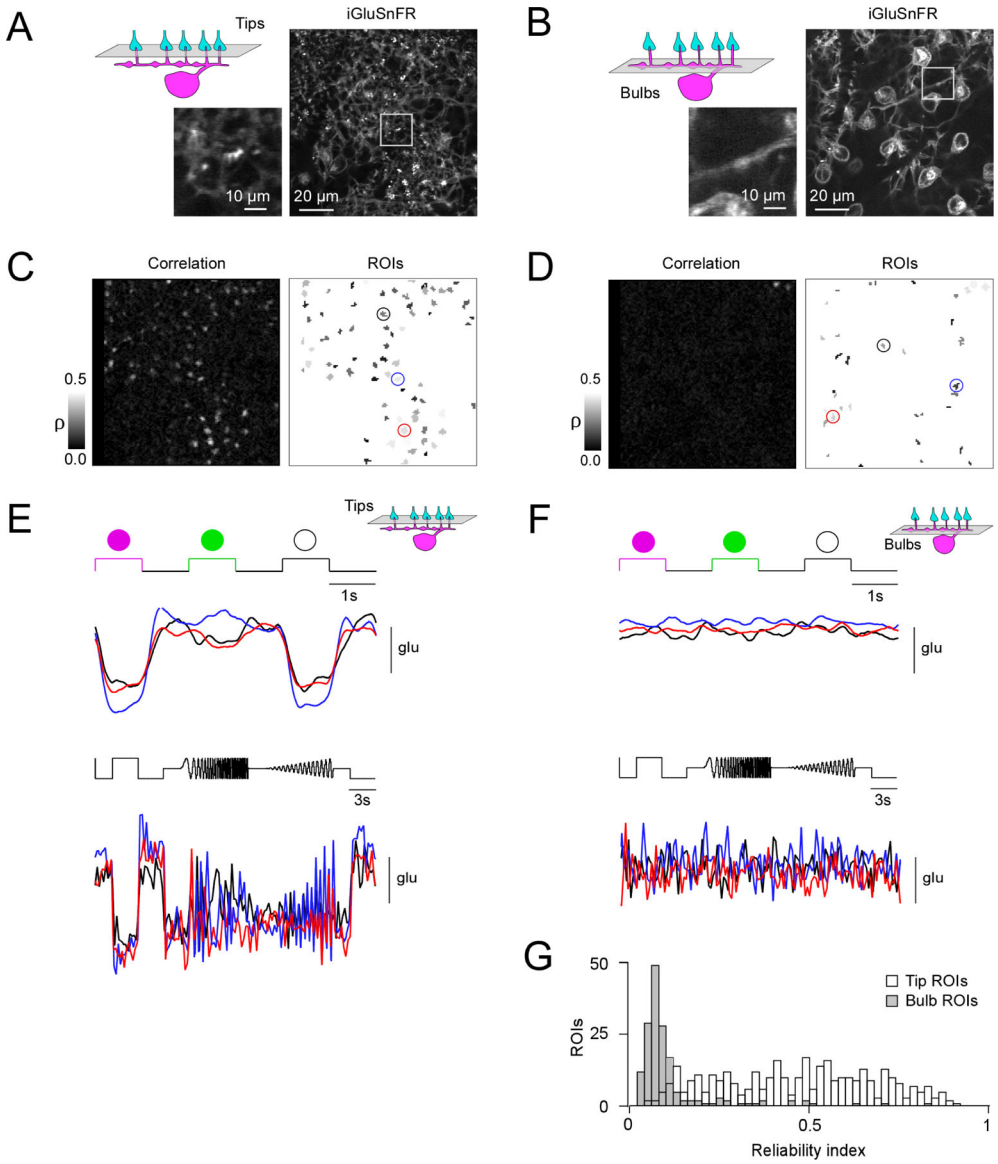

Figure 5. Glutamate imaging in the OPL

(A, B) Horizontal scans of a Cx57$^{cre/+}$ transgenic mouse retina in which HCs express the fluorescent glutamate sensor iGluSnFR after intravitreal AAV injection (see STAR Methods), with the focal plane in the OPL at the level of the HC tips (A) and at the level of the HC primary dendrites (B). (C) Correlation image (left) indicating hotspots of light-evoked glutamate release at HC tips and resulting regions-of-interest (ROIs; right). (D) Like (C) but at the primary HC dendrite level. Note that a lower correlation threshold was used than in (C) to draw ROIs (see STAR Methods). (E, F) Light-evoked glutamate signals (top, UV-green-white flashes; bottom, local chirp) are only detectable in the plane of the HC tips (E) but not at bulbs (F). (G) Histogram of reliability indices of UV-green-white flash responses for all ROIs (n = 359 at tip level, white bars; n = 166 at bulb level, grey bars) in n = 6 scan fields and n = 3 mice. $P < 0.05$; two-sided Wilcoxon rank-sum test. For complemental axial (x-z) scans see Figure S4.

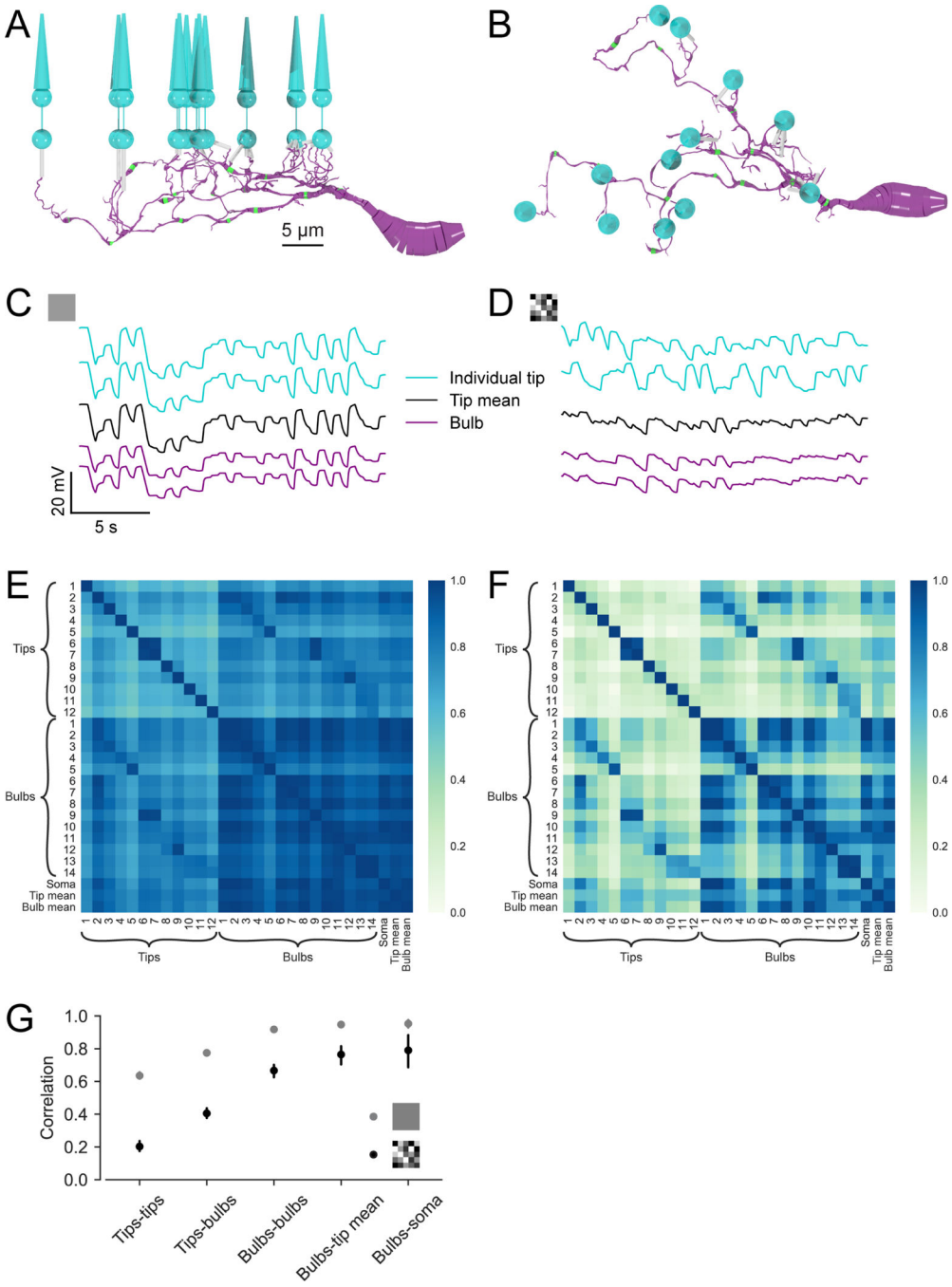

Figure 6. Biophysical modeling of the signal available at HC bulbs

(A) Side and (B) top view of the modelled HC dendrite with bulbs (green) and cones (cyan). (C, D) Examples of simulated voltage traces recorded at HC dendritic tips below cones, at bulbs and the average over all tips for (C) a random full-field noise stimulus and (D) a random checkerboard noise stimulus, for presentation purpose without synaptic vesicle release noise. (E, F) Correlations from 60 s of (E) full-field and (F) checkerboard stimulation including synaptic vesicle release noise. (G) Mean correlations between different tips, between tips and bulbs, between different bulbs, bulbs and the tip mean and bulbs and

the soma for both stimuli, see also Figure S5. Error bars show 95%-confidence intervals. See Table S2 for model parameters.

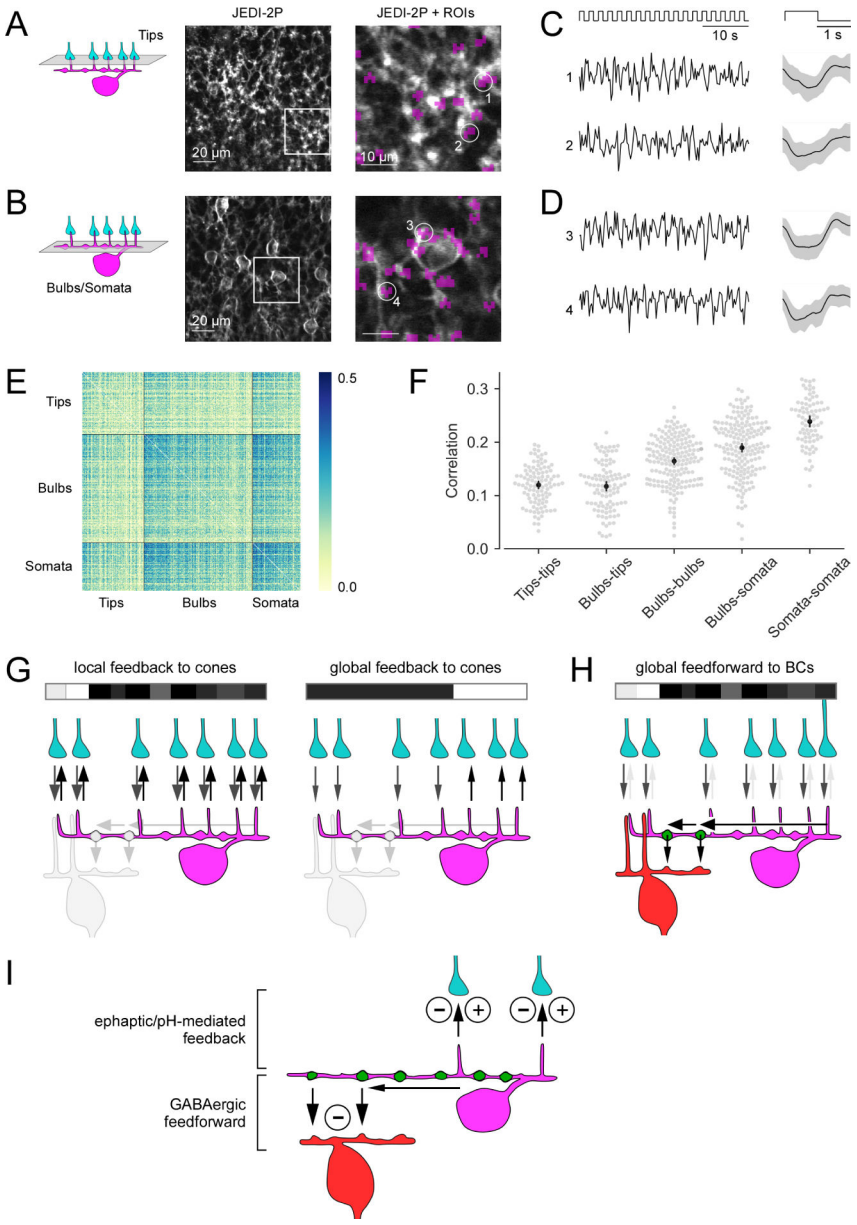

Figure 7. Voltage imaging in the OPL and bilayered synaptic circuitry of horizontal cells in the outer mouse retina

(A, B) Horizontal (x-y) scans of a Cx57$^{cre/+}$ transgenic mouse retina in which HCs express the fluorescent voltage sensor JEDI-2P after intravitreal AAV injection (see STAR Methods), with the focal plane in the OPL at the level of the HC tips (A) and of the primary dendrites (B). Right: zoomed-in images of the boxed areas. Regions-of-interest (ROIs, purple) were defined by correlation between neighboring pixels, with ROI size clamped to max. 3 µm in diameter. At the primary dendrite level, ROIs were manually sorted into somata (e.g., ROI 3) and bulbs (e.g. ROIs 1, 2, 4). (C, D) Voltage responses (left, single trials; right, averages with s.d. shading) of representative ROIs to full-field white flashes, with the focal plane in the OPL at the level of the HC tips (C) and at the level of the primary dendrites (D). (E) Correlations between single trials of tips (n = 104), bulbs (n =

181) and somata (n = 80). (F) Mean correlations within and between ROI types. Each dot in the swarm plots (gray) corresponds to one ROI and shows its mean correlation with all ROIs of the reference ROI type (mentioned first in the x-axis labels). Black: Mean +-95%-confidence interval. Except for tips-tips vs. tips-bulbs, all neighboring groups of correlations are significantly different (permutation test, all significant p's < 0.001, see STAR Methods). (G) Dendritic tips of a HC (magenta) receive cone input (grey arrows) and provide local, cone-specific feedback (black arrows) to cone axon terminals (cyan) in the presence of a spatio-temporally uncorrelated white noise stimulus (white/grey/black bar) (left). For a more spatially correlated stimulus patterns, the feedback to cones may contain a global component (right; local feedback component not shown). (H) For an uncorrelated stimulus (like in G, left), the cone input signals (grey arrows) are integrated in the HC dendrite (black arrow) and forwarded as a global signal by a BC-contacting bulb (green) to the BC (red) forming their surround signal. (I) Illustration of the two synaptic computations performed by HCs at the two distinct OPL strata: Ephaptic/pH-mediated negative and positive feedback (minus/plus symbols) to cone axon terminals in the outer OPL and inhibitory GABAergic feedforward synapses (minus symbol) from HC bulbs to BCs in the inner OPL. GABAergic auto-synapses at the distal dendritic tips of HCs [11] are not shown. Black arrows indicate HC synaptic output.

Key resources table

REAGENT or RESOURCE	SOURCE	IDENTIFIER
Antibodies		
Anti-GABA ρ2 Receptor (GABRR2) Rabbit Polyclonal Antibody	Alomone Labs	Cat# AGA-007
Anti-Secretagogin, Sheep Polyclonal Antibody	BioVendor	Cat# RD184120100
Bacterial and virus strains		
AAV2.7m8.hSyn.iGluSnFR	D. Dalkara, Institut de la Vision, Paris, France	
AAV2/1-eF1α-DIO-JEDI-2P	F. St-Pierre, Department of Neuroscience, Baylor College of Medicine, Houston, USA	
Chemicals, peptides, and recombinant proteins		
Alexa Fluor 568 hydrazide	Thermo Fisher	Cat# A10437
Deposited data		
Jupyter notebooks, analysis scripts and data	This paper	https://github.com/berenslab/hc-connectivity
SBEM dataset e2006	[22]	https://www.neuro.mpg.de/connectomics
Experimental models: Organisms/strains		
Wildtyp mouse line: C57BL/6J	The Jackson Laboratory	Stock No: 000664
Transgenic mouse line: Cx57$^{cre/+}$	Own breeding colony	Ströh et al (2013). PLoS One *8*, 15–17
Software and algorithms		
KNOSSOS 5.1	[60]	www.knossos.app
FIJI	[63]	https://imagej.net/software/fiji/
Scan M	M. Müller, MPI for Neurobiology; and T. Euler	NA
IGOR Pro 6.3	Wavemetrics	https://www.wavemetrics.com/products/igorpro
Python 3.8		https://www.python.org/
R		https://www.r-project.org/
Vaa3D	[61]	https://alleninstitute.org/what-we-do/brain-science/research/products-tools/vaa3d/
NeuronC 6.3.50	[48]	http://retina.anatomy.upenn.edu/~rob/neuronc.html